nature communications

Article

https://doi.org/10.1038/s41467-025-61117-1

Revealing umbrella bending as a reporter mode in the D+CH_4 reaction

Received: 2 February 2025

Accepted: 12 June 2025

Published online: 01 July 2025

Check for updates

Yuxin Tan[1,7], Bin Zhao[2,3,7] ✉, Daofu Yuan[4,7], Fan Li[1], Shanshan Yu[1], Mengda Jin[1], Yu Zhang[1], Chang Luo[1], Wentao Chen[1], Tao Wang[2], Jikai Zhu[2], Ziwei Wang[2], Tiangang Yang[2], Shu Liu[5], Uwe Manthe[3], Xingan Wang[1,6] ✉, Dong H. Zhang[5,6] ✉ & Xueming Yang[2,5,6] ✉

How the non-reacting moiety of a molecule influences a polyatomic reaction has been a topic of much research interest. Here we present a comprehensive investigation of the D + CH_4 → HD + CH_3 reaction, a benchmark polyatomic elementary reaction with CH_3 as the non-reacting moiety, employing a high-resolution crossed molecular beams apparatus and an accurate seven-dimensional wave packet method. An interesting angular distribution of the $CH_3(v'=1)$ product umbrella bending vibrational state is observed to scatter more in the sideways direction than the $CH_3(v'=0)$ one. By monitoring the wave functions on a dividing surface in the transition state region, the CH_3 umbrella bending mode is established as a reporter mode that faithfully reveals how the D atom dynamically approaches CH_4 at different total angular momenta or impact parameters. This discovery of the reporter mode provides an opportunity for the detailed study of polyatomic reaction dynamics.

During the transient breaking and forming of chemical bonds, chemical reactions have never shown a lack of fascinating dynamical processes. The discovery and understanding of these interesting dynamics often result from the introduction of concepts, such as dynamical resonance,[1] quantum interference,[2,3] and the geometric phase effect,[4,5] which have served as the building blocks of the detailed physical picture of the dynamical reaction processes.

Polyatomic reactions are characterized as chemical processes involving more than three atoms in reaction dynamics studies, but only a small number of the atoms are actively involved near the reaction site, and the remaining moieties of the molecules are non-reacting. The synchronized collective motions of the atoms in a molecule are called vibrational normal modes. In polyatomic reactions, there are multiple vibrational normal modes, and some involve both the reactive and non-reacting parts of the molecules. Excitation of different vibrational modes results in different efficacies in promoting the reaction process, which is commonly referred to as mode specificity and bond selectivity.[6–8] According to their roles in the reaction process, vibrational modes are often grouped into two categories: active modes and spectator modes, and the former can be further classified as reactive (promoting) modes, transitional modes, and adiabatic modes.[9,10] However, how the non-reacting moieties influence the overall reaction is still not fully understood.

The detailed understanding of chemical reactions relies on accurate experimental measurements and high-level theoretical calculations, which provide insightful information on the state-to-state reaction dynamics.[6,7,11,12] Angular distributions of specific product quantum states, namely the quantum state-specific differential cross sections (DCSs), reveal indirectly the most intricate dynamical information from a sophisticated analysis. It would be beneficial if the dynamical processes could be directly monitored. However, chemical reactions proceed very fast, and the direct experimental observation

[1]State Key Laboratory of Chemical Reaction Dynamics and Department of Chemical Physics, University of Science and Technology of China, Hefei, China. [2]Department of Chemistry, College of Science, Southern University of Science and Technology, Shenzhen, China. [3]Theoretische Chemie, Fakultät für Chemie, Universität Bielefeld, Bielefeld, Germany. [4]Hefei National Research Center for Physical Science at Microscale, University of Science and Technology of China, Hefei, China. [5]State Key Laboratory of Chemical Reaction Dynamics, Dalian Institute of Chemical Physics, Chinese Academy of Sciences, Dalian, China. [6]Hefei National Laboratory, Hefei, China. [7]These authors contributed equally: Yuxin Tan, Bin Zhao, Daofu Yuan.
✉e-mail: zhaobin@sustech.edu.cn; xawang@ustc.edu.cn; zhangdh@dicp.ac.cn; xmyang@dicp.ac.cn

of the underlying process of gas-phase reactive scattering is challenging. Nonetheless, spectroscopy studies provide an enlightening concept of the reporter mode.[13–15] For example, the vibrational fingerprint mode of the 11-*cis* retinal chromophore of the visual receptor rhodopsin undergoes a frequency change during the isomerization process. Monitoring the frequency change in the reporter modes reveals the dynamic nuclear structural change.

The concept of the reporter mode is rarely mentioned in the context of bimolecular reactive scattering experiments. It is partly due to the difficulty in defining the time origin of the scattering event. Furthermore, the most studied tri-atomic reactions do not show such a reporter mode because there is only one bond to be broken and one bond to be formed. The vibrational mode that resembles the breaking of an old bond and forming of a new one at the transition state is called the reactive mode, which is closely correlated to the reactive normal mode at the transition state,[16,17], i.e., the reaction coordinate with an imaginary frequency. It exists in all chemical reaction systems regardless of the number of involved atoms. Besides the reactive mode, polyatomic reaction systems show other vibrational modes. It would be helpful if a reporter mode could be revealed to document the reaction dynamics and provide additional insights into the reaction mechanism.

The $X + CH_4 \rightarrow HX + CH_3$ (X = H, O, F, Cl, etc.) reaction and their isotopologues are among the most widely studied polyatomic reaction systems. Interestingly, most of the experimental studies focused on the reaction of methane with O, F, and Cl atoms.[7,18–25] The reactions with H atoms are rarely studied,[26–32] presumably due to the exceedingly small reactive signals. Fortunately, theoretical studies have now advanced to perform high-dimensional calculations of the $H + CH_4$ reaction at the most detailed state-to-state level.[33–37] Undoubtedly, the $H + CH_4$ reaction is the benchmark polyatomic reaction, just as the triatomic $H + H_2$ reaction. Although no bonds will be broken in the non-reacting CH_3 fragment, it is interesting to study how the vibrational modes of this fragment influence the reaction dynamics.

Evidence has been gathered to show that most of the vibrational modes of the CH_3 moiety are spectators,[27,38,39] which are not actively involved in the reaction and have negligible coupling with the reaction coordinate. Energy deposited in the spectator mode is sequestered during the reaction process, and their excitations have almost no effect on the reaction. However, the umbrella bending mode of the reaction is clearly not a spectator. In an early study of the CH_3I photodissociation, the accompanying umbrella bending excitation with a long C–I stretching overtone progression suggested the correlation between the dissociation coordinate and umbrella bending coordinate.[40] Recent studies have shown that the deferred umbrella bending motion in the $H + CH_4$ substitution reaction results in a higher dynamical barrier.[41] In addition, in the $H + CHD_3 \rightarrow H_2 + CD_3$ reaction, counter-intuitive vibrational excitation of the CD_3 umbrella bending mode has been observed,[35] which revealed the active control of the reaction pathways by vibrational excitations of the CHD_3 reactant. These results apparently suggest the features of the umbrella bending mode in this polyatomic reaction.

The CH_3 umbrella bending mode appears very intriguing. It is apparently an active mode, but it cannot be directly classified into the three existing classes of active modes.[9,10] The CH_3 umbrella bending mode is not a reactive mode because the C-H bonds in the non-reacting CH_3 moiety are not broken; furthermore, it is not an adiabatic mode neither because the initial vibrational quantum deposited in this mode is not adiabatically preserved during the reaction; at last, it is not a transitional mode because theoretical calculations show negligible transfer of energy from the excited umbrella bending mode to the rotational motion of the products. In the present work, we intend to reveal the CH_3 umbrella bending mode as a reporter mode, which is shared by the CH_4 reactant and the CH_3 product and monitors the underlying dynamics on the way from reactants to products.

Here, we performed detailed experimental and theoretical studies of the angular distributions of the CH_3 product states in the $D + CH_4 \rightarrow HD + CH_3$ reaction at different collision energies, with the aim of revealing the role of the umbrella bending mode. This $D + CH_4$ reaction was chosen for its relatively larger cross section among other isotopologues. A high-resolution crossed molecular beams apparatus was employed in the current experiment to detect the small reactive signal. Velocity map images[42,43] in combination with a (2 + 1) resonance-enhanced multiphoton ionization (REMPI) scheme[18,32] were used to detect the vibrational state-selected CH_3 products. This crossed molecular beams method allowed us to obtain accurate product distributions of kinetic energy and vibrational state-specific DCSs.[44] Theoretical quantum dynamics studies employed a seven-dimensional (7D) time-dependent wave packet method and a model Hamiltonian developed by Palma and Clary.[45] Detailed DCSs were calculated with the reactant-product decoupling method.[46]

Results

The crossed molecular-beam experiment of the $D + CH_4 \rightarrow HD + CH_3$ reaction was performed on the apparatus shown in Supplementary Fig. 1. Two CH_3 product vibrational states, the ground $CH_3(v' = 0)$ state and umbrella bending excited $CH_3(v' = 1)$ state, were probed by employing the (2 + 1) REMPI ionization method, and the measured images are shown in Fig. 1a, b, d, e, g, h, respectively, at the collision energies of 0.66, 0.99, and 1.55 eV. The Newton diagram of this reaction is depicted in Fig. 1b, e, h by red lines. "F" and "B" represent the forward and backward scattering directions of the CH_3 product in the center-of-mass frame, respectively. The CH_3 products are dominantly distributed in the backward and sideways scattering directions for all experimental images. The main experimental noises were from the incident CH_4 beam, which can be seen as a circular area in the forward scattering direction. At the three selected collision energies, the boundaries between reactant beam noises and the CH_3 product signals are well separated, which allows us to derive an accurate angular distribution of the CH_3 product states. It should be noted that the reactant beam noises are ubiquitous in the $X + CH_4 \rightarrow HX + CH_3$ (X = H, O, F, Cl, etc.) reactions if the CH_3 products are detected. The noises in Fig. 1 were substantial because of the exceedingly weak reactive signals of the title reaction, which poses challenges in detailed experimental studies of this reaction. The total product translational energy distributions at the collision energies of 0.66, 0.99, and 1.55 eV were derived and presented in Supplementary Fig. 2 by integrating the experimental images in Fig. 1 along the angular coordinate, which are in very good agreement with the theoretical results.

The quantum state-specific DCS reflects crucial and detailed dynamical information. After integrating the radial part of the images of the $CH_3(v' = 0)$ and $CH_3(v' = 1)$ products in Fig. 1, the experimentally measured angular distributions of $CH_3(v' = 0, 1)$ were extracted and shown together with the theoretically calculated results in Fig. 1c, f, i. The experimental results in the forward scattering direction were not presented due to the noise from the CH_4 beam. The experimental and theoretical results are in very good agreement, suggesting the high precision of the measurements and calculations. At the collision energy of 0.66 eV, the CH_3 products show a dominantly backward distribution, and the distribution gradually decreases towards smaller scattering angles. At the collision energies of 0.99 and 1.55 eV, the CH_3 products scattered to a wider angular range when more energy became available. Most interestingly, the $CH_3(v' = 1)$ products were distributed more to the sideways direction than the $CH_3(v' = 0)$ one at all three collision energies.

Discussion

Angular distributions of product states are closely related to mode specificity and bond selectivity. The latter studies the influence of reactant vibrational excitations on the control of chemical reaction

https://doi.org/10.1038/s41467-025-61117-1

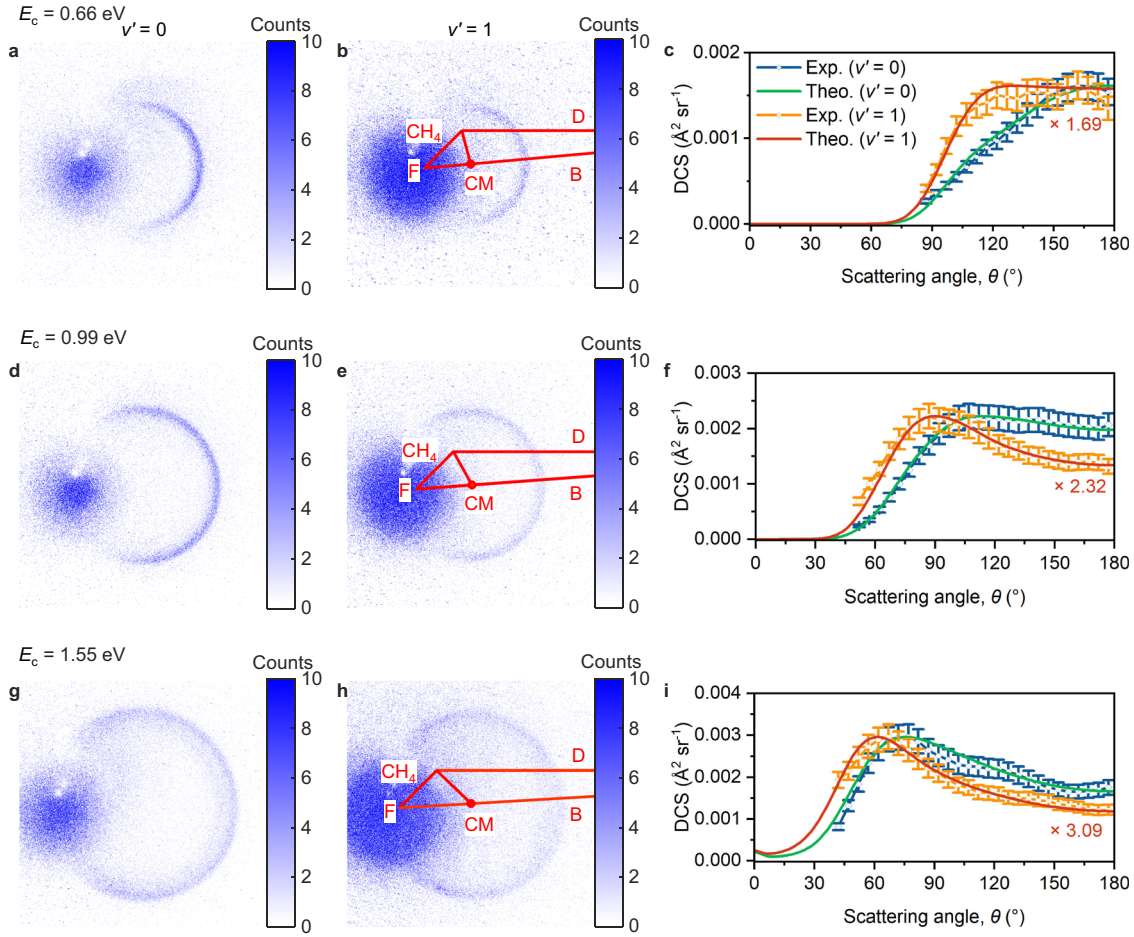

Fig. 1 | Experimental images and vibrational state-specific angular distributions. a Experimental time-sliced velocity map image of $CH_3(v'=0)$ products at a collision energy of 0.66 eV. The color scale represents the ion counts of CH_3^+. **b** The experimental time-sliced velocity map image of $CH_3(v'=1)$ products at a collision energy of 0.66 eV. The Newton diagram for the D + CH_4 reactive scattering is depicted by red lines. The "CH_4" and "D" denote the directions of the two reactant beams. "F" and "B" denote the forward and backward scattering directions corresponding to the incident CH_4 beam in the center-of-mass (COM) frame. "CM" denotes the center of mass for reactive scattering. **d**, **e** The same as (**a** and **b**), except at a collision energy of 0.99 eV. **g**, **h** The same as (**a** and **b**), except at a collision energy of 1.55 eV. **c**, **f** and (**i**)The experimental (Exp.) and calculated (Theo.) differential cross sections (DCSs) at collision energies of 0.66, 0.99, and 1.55 eV, respectively, in units of Å² sr^{-1}, in which sr stands for steradian. The experimental DCSs for $CH_3(v'=0)$ and $CH_3(v'=1)$ products are plotted in dark blue and bright orange, while the calculated DCSs for $CH_3(v'=0)$ and $CH_3(v'=1)$ products are plotted in dark cyan and strong red. To better present the different angular distributions of the $v'=0$ and 1 product states at each collision energy, the DCS of the $v'=1$ product is scaled to a similar amplitude as the $v'=0$ product. 0 and 180° represent the forward and backward scattering directions, respectively. The counting events were about 500,000 laser shots for the $CH_3(v'=0)$ reaction channel, while the counting events were about 2,000,000 laser shots for the $CH_3(v'=1)$ reaction channel. The error bars for experimental DCSs are estimated to be about 10%, which mainly comes from the uncertainty of experimental measurement and the fitting process. Source data are provided as a Source Data file.

when reactants proceed toward the transition state region, and the former studies energy decomposition and angular distribution of product states when products move away from the transition state region. Due to the micro-reversibility of elementary reactions, the two types of studies both help to reveal the underlying dynamics of polyatomic reaction systems. Resolving product CH_3 umbrella bending states and angular distributions provides detailed information on the underlying dynamics.

It is very interesting to observe a more sideways distributed angular distribution of the $CH_3(v'=1)$ vibrational state than the $CH_3(v'=0)$ one in Fig. 1. Common wisdom would expect the opposite angular distribution. The title reaction features a colinear transition state and proceeds through a rebound mechanism: the incoming D atom abstracts an H atom from the CH_4 reactant, and the HD product rebounces to the opposite direction. The CH_3 product also rebounces in the opposite direction to the incoming CH_4 reactant. This mechanism would expect more vibrational excitation in the backward direction at moderate collision energies because collisions with low-impact parameters transfer much energy into vibrations, and the vibrationally excited products would be mainly back-scattered.[47] Apparently, the angular distribution of the $CH_3(v')$ vibrational states in Fig. 1 defies this expectation and contains interesting dynamical information on the title reaction.

Product angular distributions and opacity functions

First of all, the $CH_3(v'=0, 1)$ product angular distributions are closely related to the opacity function, which is a concept used to describe the reaction probabilities as a function of the total angular momentum, J_{tot}, in a quantum sense (or the corresponding classical impact parameter, i.e., the perpendicular distance, b, between the paths of the colliding particles if they were to continue without interacting). Without losing generality, results at the collision energy of 0.99 eV are selected to analyze in detail in Fig. 2, and the results at the other two collision energies can be found in Supplementary Figs. 8, 9. The results for the $CH_3(v'=0)$ and $CH_3(v'=1)$ products are plotted as the blue and green lines, respectively, in Fig. 2a. The plots provide insights into how

https://doi.org/10.1038/s41467-025-61117-1

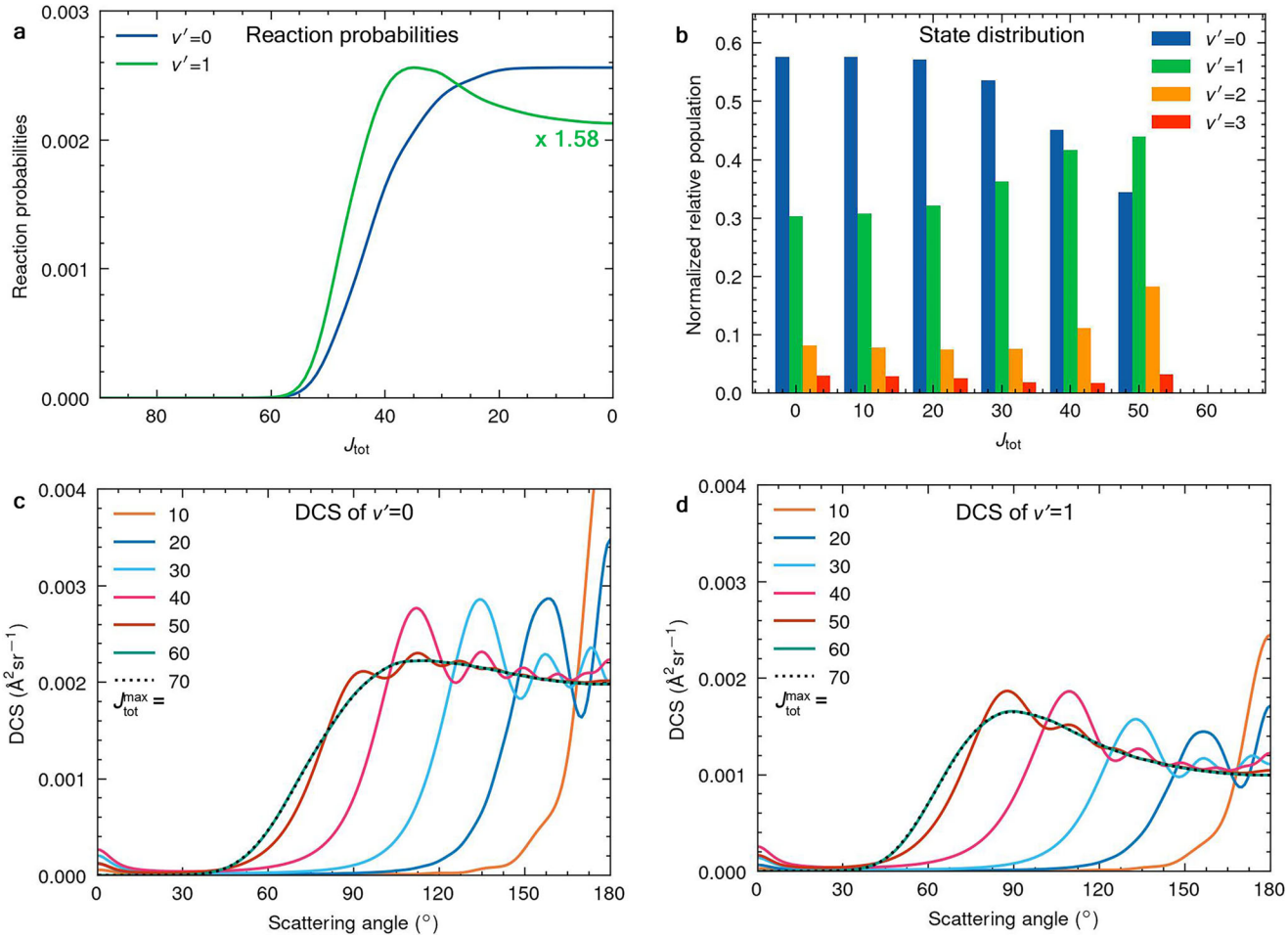

Fig. 2 | Analysis of the angular distributions of the ground $CH_3(v'=0)$ and umbrella bending excited $CH_3(v'=1)$ product states at the collision energy of 0.99 eV. a Reaction probabilities as a function of the total angular momentum, J_{tot}, for the two product states. **b** Normalized relative populations of the CH_3 umbrella bending vibrational states at different J_{tot}'s. The population of the $v'=1$ state increases with the increasing J_{tot}. **c** Differential cross section (DCS) of the $CH_3(v'=0)$ product state calculated with different values of J_{tot}^{max}, in units of Å^2 sr^{-1}, in which sr stands for steradian. **d** The same as c but for DCS of the $CH_3(v'=1)$ product state. The backward scattering direction of the DCS has the largest contribution from small partial waves, and the scattering direction shifts to the sideways and forward directions when more partial waves contribute to the reaction processes. Similar results for the collision energies of 0.66 and 1.55 eV are shown in Supplementary Figs. 8, 9, respectively. Source data are provided as a Source Data file.

likely the reaction is to occur at different total angular momenta. The $CH_3(v'=0)$ state shows a decreased reaction probability with an increased J_{tot}, while the $CH_3(v'=1)$ one peaks at about $J_{tot}=35$. This indicates a tendency of forming the $CH_3(v'=1)$ products at large J_{tot}, which are shown in Fig. 2b for six selected J_{tot}'s. At each J_{tot}, the probabilities of forming all the CH_3 vibrational states are normalized to be 1.0. It is clear that $CH_3(v'=0, 1)$ are the two main vibrational states, and the remaining ones are negligible for all J_{tot}'s. Although the data in Fig. 2a, b is plotted differently, it shows the same tendency of forming the umbrella excited CH_3 state with increasing J_{tot}'s.

As we know, different partial waves, J_{tot}'s, contribute to specific directions of the DCS. For example, for direct reactions without deep trapping wells, the backward scattering direction of the DCS has the largest contribution from small partial waves, and the scattering direction shifts to the sideways and forward directions when more partial waves contribute to the reaction processes. One important exception is the dynamical resonance, in which the reaction intermediate is transiently trapped and the recoiling products are eventually scattered in the forward direction after a certain amount of rotation during the surviving period. The title reaction is a direct reaction without featuring any trapping well along the reaction path (see Supplementary Fig. 4). Thus, the backward and sideways signals in Fig. 1 can be attributed to the small and large partial waves, respectively. Figure 2c, d shows DCSs calculated with different J_{tot}^{max}, the maximum value of J_{tot}, for the $CH_3(v'=0)$ and $CH_3(v'=1)$ product states, respectively. With the increasing J_{tot}^{max}, the DCSs shift more to the sideways direction. In particular, the peak of the $CH_3(v'=1)$ DCSs emerges only when roughly the $J_{tot} \approx 0$-50 partial waves are included. These results align well with the expectations of a direct reaction.

Revealing the CH3 umbrella bending mode as a reporter mode

To understand the interesting angular distribution and vibrational state population of the umbrella bending mode of the CH_3 product, the topography of the potential energy surface (PES) merits some analysis because it illustrates important features of the reactants, transition state, and products. The three most relevant coordinates are defined in Fig. 3a: R is the distance between the CH_4 center of mass and the D atom, and r is the distance between the center of mass of the non-reacting CH_3 moiety and the reacting H atom; the CH_3 umbrella bending coordinate χ is the angle between the C_{3v} symmetry axis of the non-reacting CH_3 moiety and any of the non-reacting C-H bond. A more detailed description of the coordinates of the 7D model Hamiltonian, 2D plot of the PES along the reaction coordinate, and 1D cuts of

https://doi.org/10.1038/s41467-025-61117-1

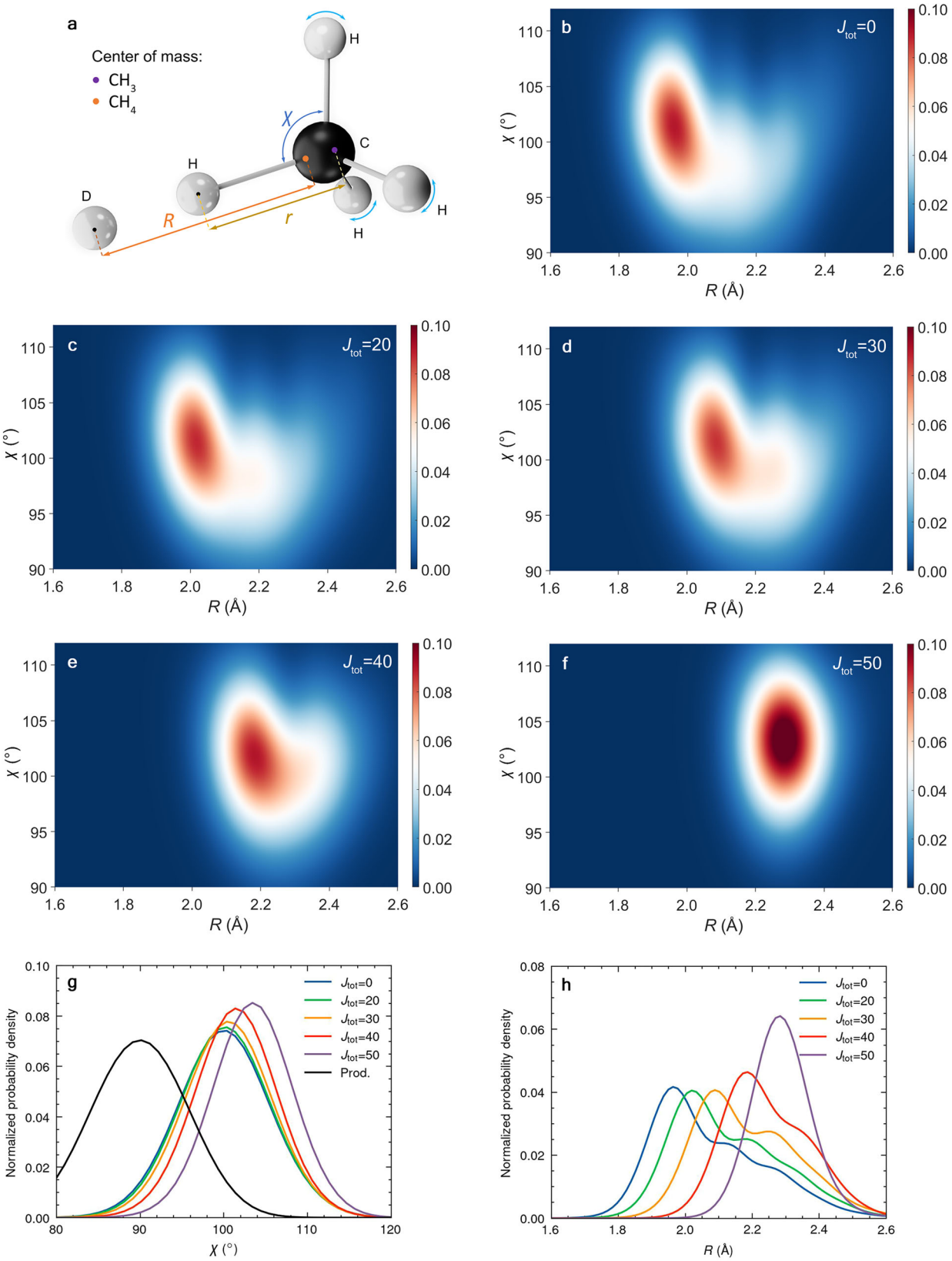

the potential are given in the Supplementary Figs. 3, 4. It is interesting to highlight the change of the CH_3 umbrella bending mode while the reactive flux passes from reactants to products. The umbrella bending mode exists in both the CH_4 reactant and the CH_3 product, but the equilibrium geometry and the vibrational frequency of this mode undergo a dramatic change along the reaction path. In the reactant $D + CH_4$ asymptotic region, the minimum of the umbrella bending potential features a value of 109.5°, and it gradually changes to 90° in the product $HD + CH_3$ asymptotic region. At the same time, the vibrational frequency decreases from 1330 to 600 cm^{-1}.

Thanks to the dynamic correlation of the vibrational frequency and the equilibrium geometry to the reaction coordinate, the CH_3

Fig. 3 | Coordinate definitions and plots of the reactive scattering wave functions at the collision energy of 0.99 eV. a Definition of the three most relevant internal coordinates, R, r, and the umbrella bending angle χ. The wave functions on the dividing surface at $r = 1.59$ Å are projected onto the R coordinate and the umbrella bending χ coordinate. **b**–**f** 2D probability densities of wave functions of $J_{tot} = 0$, 20, 30, 40, and 50. The shapes of the wave functions change with increasing J_{tot}'s. A more detailed view of the variation of the wave functions is given in Supplementary Movie 2. (Each frame of the movie is the wave function of a J_{tot}). **g** 1D wave functions in the umbrella bending χ coordinate after integrating the 2D wave functions in the R coordinate. With increasing J_{tot}, the 1D wave functions shift further away from the ground vibrational state of the CH_3 product (denoted by the black curve). **h** 1D wave functions in the R coordinate after integrating the 2D wave functions in the umbrella bending χ coordinate. With increasing J_{tot}, the 1D wave functions shift further to large R-values, i.e., larger distance between the D atom and the CH_4 molecule. Similar results for the collision energies of 0.66 and 1.55 eV are shown in Supplementary Figs. 10, 11, respectively. Source data are provided as a Source Data file.

umbrella bending mode is promising to provide a probing tool for the underlying reaction dynamics. In the title reaction, the attacking of the D atom to the CH_4 molecule and the departure of HD and CH_3 products proceed very fast, thus the vibrational state of the CH_3 umbrella bending mode cannot adiabatically follow the motion in the reaction coordinate and results in multiple vibrational excitations, as shown in Fig. 2. Due to this interesting behavior, the umbrella bending mode acts as a reporter mode in the title reaction, and the different angular distribution of the $CH_3(v' = 0)$ and $CH_3(v' = 1)$ states in Fig. 1 encloses interesting dynamical information.

Dynamics reported by the CH3 umbrella bending mode

To reveal how the umbrella reporter mode monitors the reaction process is an intriguing pursuit. It is well-known that the transient wave functions near the transition state entail all the dynamical information on the reaction process. The reaction barrier features a geometry with an r-value of 1.43 Å in contrast to the equilibrium value of 1.16 Å in the CH_4 reactant. A dividing surface at $r = 1.59$ Å (denoted as a dashed green line in Supplementary Fig. 4a) is located near the product side of the transition state and thus can be used to analyze the reactive wave function. Once traversing this dividing surface, the wave function proceeds directly to the product region and never returns to the transition state region. In Fig. 3b–f, energy-dependent scattering wave functions on this dividing surface are shown for five selected partial waves (Supplementary Movie 2 shows the animated change of the wave functions, with each frame representing the wave function of a partial wave.). The collision energy is selected to be 0.99 eV, and the results of the other collision energies are shown in Supplementary Figs. 10 and 11. In each figure, the wave function shows a correlation between the χ and R coordinates: the wave functions tilt to a small χ region for large R-values. This is because a large R value on the dividing surface represents not only a large D and CH_4 distance but also a large separation of the HD and CH_3 products. The departure of the HD and CH_3 products results in an increased value of the R coordinate. Thus, the wave functions are in accordance with the decreasing equilibrium geometry of the χ coordinate along the reaction path towards products.

The change of the umbrella wave function with respect to J_{tot} is more interesting. Figure 3g shows the wave functions in the umbrella bending χ coordinate after integrating the wave functions in the R coordinate. These 1D scattering wave functions of different partial waves show interesting patterns: the larger the partial wave is, the more the scattering wave function differs from the ground vibrational state of the CH_3 product (denoted by the black curve), which suggests that the CH_3 product is vibrationally excited. The variations of the wave functions with respect to J_{tot} are not dramatic, but the corresponding effects on the CH_3 product vibrational state distribution are significant, which had also been observed in the vibrational control of the reaction pathway in the $H + CHD_3 \rightarrow H_2 + CD_3$ reaction.[35]

As a reporter mode, the shapes of the CH_3 umbrella bending wave functions for different J_{tot}'s are capable of reporting the dynamic approach of the D reactant to the CH_4 molecule. For nonzero partial waves, the orbital angular momentum exerts on the rotating reactive system a centrifugal repulsion force that impedes the approaching of the D atom to the CH_4 reactant; thus, for larger partial waves, the reactive H atom is abstracted by the D atom at a larger R distance, as shown in Fig. 3h for the wave functions in the R coordinate after integrating the wave functions in the χ coordinate. At a larger R distance, the wave function in the χ coordinate is less disturbed by the incoming D atom and resembles more the one in CH_4. As the CH_4 reactant shows a larger equilibrium value of χ than the CH_3 product, it is now not difficult to rationalize that the CH_3 umbrella bending wave functions shift more to a large χ value for large J_{tot}'s.

Dynamic approach of D to CH4 at different partial waves

In the end, the schematic of the CH_3 umbrella bending reporter mode in the title reaction is displayed in Fig. 4. The total angular momentum, J_{tot}, of the reactive system is quantized in the quantum sense, and the corresponding classical counterpart is the impact parameter b, which is the perpendicular distance between the paths of the colliding D atom and CH_4 molecule if there were no interaction between them. The vertical axis of Fig. 4 denotes J_{tot} and can thus be considered as the impact parameter b. For different J_{tot}'s, the D atom approaches the CH_4 molecule with different impact parameters. Due to the centrifugal repulsion force at larger impact parameters, the D atom abstracts an H atom from CH_4 at increasingly bigger values of the R coordinate, which are indicated by the colored circular rings in Fig. 4. The corresponding 1D wave functions, $\psi(\chi)$, and the vibrational state populations of the CH_3 umbrella bending mode are shown on the top right corner. The shapes of the wave functions can report the dynamic approach of the D atom to CH_4, but the wave functions can not be directly observed in the experiment. Nevertheless, the angular distributions of the $CH_3(v' = 0)$ and $CH_3(v' = 1)$ products in the measured and calculated DCSs in Fig. 1 encode the dynamics of the reaction. The 1D wave functions of increasing J_{tot} shift more to larger χ values (further away from the ground state product), which suggests more vibrational excitation for larger J_{tot}. Vibrationally excited product umbrella bending states have more contribution from larger partial waves and thus show a more sideways and forward angular distribution, which is exactly shown in Fig.1.

In conclusion, combined experimental and theoretical studies found that the $CH_3(v' = 1)$ product states in the $D + CH_4 \rightarrow HD + CH_3$ reaction were distributed more to the sideways direction than the $CH_3(v' = 0)$ state at three selected collision energies, which has been analyzed by following umbrella bending wave functions of different partial waves and has revealed the CH_3 umbrella bend as a reporter mode. This CH_3 umbrella bending reporter mode reveals the dynamic approach of the D atom to CH_4 at different partial waves, which is in perfect accordance with the well-understood role of the centrifugal force in chemical reactions. Wave functions of larger partial waves are found to shift more to large χ values, i.e., further away from the CH_3 equilibrium value, and thus, the CH_3 product is more vibrationally excited for larger partial waves. As a result, the $CH_3(v' = 1)$ product states distribute more to the sideways and forward directions in the product angular distribution.

The revealing of the umbrella bending reporter mode is expected to show a significant impact on the understanding of more detailed reaction dynamics. This mode exists in both the CH_4 reactant and the CH_3 product of the $X + CH_4 \rightarrow HX + CH_3$ reactions and gradually changes its equilibrium position and vibrational frequency along the

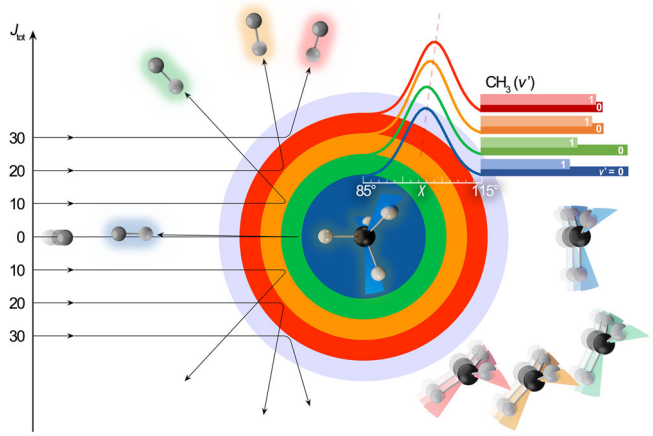

Fig. 4 | Schematic of the CH_3 umbrella bending reporter mode. The reporter mode continuously reveals how the reactant D atom dynamically approaches the CH_4 co-reactant and how the HD and CH_3 products recoil from each other. At different partial waves, the rotating reaction system experiences different centrifugal repulsion forces that impede the approach of the D atom to the CH_4 reactant. A larger J_{tot} corresponds to a larger repulsion force so that the reactive H atom is abstracted by the D atom at a larger R distance, where the wave function in the χ coordinate resembles more the one in the CH_4 reactant and differs more from the one in the CH_3 product. As a result, the relative $CH_3(v'=0)$ population decreases and the $CH_3(v'=1)$ one increases with the increasing J_{tot}. As large J_{tot} contributes more to the sideway scattering direction, the DCSs of the $CH_3(v'=1)$ product states show more sideway scattering than the $CH_3(v'=0)$ ones.

reaction path. The umbrella bending wave functions in the CH_4 reactant and the CH_3 product are the same for all the reactions, but the way how the umbrella wave function changes from the reactant to the product varies for different reactions, which is truly the fascinating part of chemical reaction dynamics. Different reactions show a variation of the exothermicity, the barrier height and geometry of the transition state, and mass combination. The CH_3 umbrella bending reporter mode thus facilitates the discovery and understanding of versatile polyatomic reaction dynamics by continuously reporting the reaction process.

At last, the discovery of an additional active mode, i.e., the CH_3 umbrella bending reporter mode in the $X + CH_4 \rightarrow HX + CH_3$ polyatomic reaction systems, not only provides insightful probing tools for the underlying complex reaction dynamics but also reveals peculiar features of vibrational control that complement classification of active modes as reactive mode, adiabatic mode, or transitional mode. An analogous reporter mode is expected to exist in other polyatomic reactions whenever the vibrational frequency and the equilibrium geometry of a vibrational mode dynamically correlate to the reaction coordinate. The revealing of the reporter mode provides a valuable opportunity for studying the versatile quantum effects in polyatomic reaction systems.

Methods

Experiment

The experiments were carried out on a crossed molecular beams apparatus combined with the time-sliced product velocity map imaging method[42,43] (see Supplementary Fig. 1). The deuterium atom beam was generated by the photodissociation of DI precursor molecules introduced by the supersonic expansion via a pulsed valve. The DI gas sample was synthesized by the reaction of red phosphorus, iodine and deuterated water in a pre-evacuated environment. The produced DI sample was collected with a gas cylinder under liquid nitrogen temperature. A KrF excimer laser (248 nm) and the fourth harmonic output of an Nd:YAG laser (266 nm) were employed as the photolysis laser. The pulse energy of the photolysis laser was ≈100 mJ. The photolysis laser was focused about 8 mm downstream from the nozzle. D atom beams with three different velocities were produced by controlling the photolysis laser polarization via polarization optics. The high-intensity CH_4 (purity: ≈ 99.9%) molecular beam was generated by the supersonic expansion of neat CH_4 via a second pulsed valve (Even-Lavie valve) at a stagnation pressure of 7 atm. After the collimation of mounted skimmers, the pulsed D-atom beam and CH_4 beam overlapped in the reaction scattering region spatially and temporally with a crossing angle of 135°. The reaction collision energies were calibrated to be 0.66, 0.99, and 1.55 eV by determining the velocities of the D-atom beam and CH_4 beam. The nascent CH_3 products from the $D + CH_4 \rightarrow HD + CH_3$ reaction were detected via a one-color (2 + 1) REMPI ionization method[18,32] by the frequency-doubled output of a tunable dye laser. The wavelength of the detection laser (≈ 7 mJ per pulse) was set to be ≈333 and 329 nm for the $CH_3(v'=0)$ and $CH_3(v'=1)$ products, respectively. Through a specially designed electrostatic lens system, the ionized CH_3 products were mapped onto a position-sensitive microchannel plate detector coupled with a phosphor screen. The raw experimental images were recorded by a scientific Complementary Metal Oxide Semiconductor (sCMOS) camera. All the timing of the entire system was controlled by three digital delay generators simultaneously at a repetition rate of 20 Hz. Typically, to acquire a well-resolved experimental image, the counting events were about 500,000 laser shots for $CH_3(v'=0)$ reaction channel, while the counting events were about 2,000,000 laser shots for $CH_3(v'=1)$ reaction channel.

Theory

Theoretical calculations were performed with the highly paralleled in-house ABR program suite for nuclear quantum dynamics of polyatomic molecular systems. This program suite is developed to study the ABR type of molecular systems, where A and B represent two individual atoms, and R is the remaining group of atoms. Specifically for the title reaction, A and B are the D and H atoms, respectively, and R is the CH_3 moiety.

The description of the CH_3 internal motion, in principle, requires six coordinates in full dimensionality, but in practice, only one coordinate should be explicitly included because the other five vibrational modes behave perfectly as spectator modes, which are not actively involved in the reaction. The model Hamiltonian developed by Palma and Clary[45] has been used in reduced-dimensional studies. The applicability and accuracy of this reduced-dimensional model have been tested in the comparison with results of full-dimensional calculations[38,39] and with experimental observation.[18] Thus, it is reasonable to see a good agreement between the experimental and theoretical results in Fig. 1, which further suggests the angular distribution in Fig. 1 is very trustworthy.

In the current seven-dimensional calculations, the non-reacting CH_3 moiety is restricted to the C_{3v} symmetry,[45] and only the CH_3 umbrella bend is explicitly considered, which is described by the χ coordinate in Supplementary Fig. 3. The umbrella angle χ is defined as the angle between the CH bond and the C_{3v} symmetry axis **s**. The remaining six coordinates and the explicit Hamiltonian are defined in detail in the Supplementary Fig. 3 of Supplementary Note 2 and in ref. 34. The calculations employed the permutationally invariant PES of ref. 48.

The present theoretical study pre-selects one of the four H atoms to be reactive, and the other three H atoms in the CH_3 moiety are non-reacting. Attentive readers may note that the four H atoms in the CH_4 reactant are all reactive in the experiment, and treating the CH_3 moiety as non-reacting would reduce the total reactivity. It should be noted that the four reactive channels are isolated. Once the D atom approaches one of the H atoms, there is no chance for the D atom to react with the other H atoms because the four equivalent transition states are separated by high barriers. Thus, the present model only

considers one of the four equivalent reactive channels, and a factor of four should be considered.

Data availability

The data that support the findings of this study are available from Figshare[49] and from the corresponding authors upon request. Source data are provided in this paper.

Code availability

The code used in this study is available from the corresponding authors upon request.

References

1. Wang, T. et al. Dynamical resonances in chemical reactions. *Chem. Soc. Rev.* **47**, 6744–6763 (2018).
2. Chen, W. et al. Quantum interference between spin-orbit split partial waves in the F + HD → HF + D reaction. *Science* **371**, 936–940 (2021).
3. Jambrina, P. et al. Quantum interference between H + D_2 quasi-classical reaction mechanisms. *Nat. Chem.* **7**, 661 (2015).
4. Yuan, D. et al. Observation of the geometric phase effect in the H + HD → H_2 + D reaction. *Science* **362**, 1289–1293 (2018).
5. Yuan, D. et al. Observation of the geometric phase effect in the H + HD → H_2 + D reaction below the conical intersection. *Nat. Commun.* **11**, 3640 (2020).
6. Crim, F. F. Vibrational state control of bimolecular reactions: discovering and directing the chemistry. *Acc. Chem. Res.* **32**, 877–884 (1999).
7. Liu, K. Vibrational control of bimolecular reactions with methane by mode, bond, and stereo selectivity. *Annu. Rev. Phys. Chem.* **67**, 91–111 (2016).
8. Jiang, B. & Guo, H. Control of mode/bond selectivity and product energy disposal by the transition state: X + H_2O (X = H, F, O(^{3}P), and Cl) reactions. *J. Am. Chem. Soc.* **135**, 15251–15256 (2013).
9. Yan, S., Wu, Y. T. & Liu, K. Tracking the energy flow along the reaction path. *Proc. Natl. Acad. Sci. USA* **105**, 12667–12672 (2008).
10. Pan, H., Zhao, B., Guo, H. & Liu, K. State-to-state dynamics in mode-selective polyatomic reactions. *J. Phys. Chem. Lett.* **14**, 10412–10419 (2023).
11. Clary, D. C. Theoretical studies on bimolecular reaction dynamics. *Proc. Natl Acad. Sci. USA* **105**, 12649–12653 (2008).
12. Zhang, D. H. & Guo, H. Recent advances in quantum dynamics of bimolecular reactions. *Annu. Rev. Phys. Chem.* **67**, 135–158 (2016).
13. Dantus, M., Rosker, M. J. & Zewail, A. H. Real-time femtosecond probing of "transition states" in chemical reactions. *J. Chem. Phys.* **87**, 2395–2397 (1987).
14. Kukura, P., McCamant, D. W. & Mathies, R. A. Femtosecond stimulated Raman spectroscopy. *Annu. Rev. Phys. Chem.* **58**, 461–488 (2007).
15. Wu, Y. C., Zhao, B. & Lee, S. Y. Time-dependent wave packet averaged vibrational frequencies from femtosecond stimulated Raman spectra. *J. Chem. Phys.* **144**, 054104 (2016).
16. Grote, R. F. & Hynes, J. T. Reactive modes in condensed phase reactions. *J. Chem. Phys.* **74**, 4465–4475 (1981).
17. Maldonado-Domínguez, M., Bím, D., Fucík, R., Curík, R. & Srnec, M. Reactive mode composition factor analysis of transition states: the case of coupled electron-proton transfers. *Phys. Chem. Chem. Phys.* **21**, 24912–24918 (2019).
18. Chen, Z. et al. Reactivity oscillation in the heavy-light-heavy Cl + CH_4 reaction. *Proc. Natl. Acad. Sci. USA* **117**, 9202–9207 (2020).
19. Wang, F. & Liu, K. P. Enlarging the reactive cone of acceptance by exciting the C-H bond in the O(^{3}P) + CHD_3 reaction. *Chem. Sci.* **1**, 126–133 (2010).
20. Zhang, B., Liu, K. P. & Czakó, G. Correlated dynamics of the O(^{3}P) + CHD_3(v = 0) reaction: a joint crossed-beam and quasiclassical trajectory study. *J. Phys. Chem. A* **119**, 7190–7196 (2015).
21. Pan, H., Liu, S., Zhang, D. H. & Liu, K. P. From reactive rainbow to dynamic resonance well. *J. Phys. Chem. Lett.* **11**, 9446–9452 (2020).
22. Lin, J. J., Zhou, J. G., Shiu, W. C. & Liu, K. P. State-specific correlation of coincident product pairs in the F + CD_4 reaction. *Science* **300**, 966–969 (2003).
23. Pan, H. L. & Liu, K. P. Fermi-phase-induced interference in the reaction between Cl and vibrationally excited CH_3D. *Nat. Chem.* **14**, 545–549 (2022).
24. Pan, H. L., Wang, F. Y., Czakó, G. & Liu, K. P. Direct mapping of the angle-dependent barrier to reaction for Cl + CHD_3 using polarized scattering data. *Nat. Chem.* **9**, 1175–1180 (2017).
25. Pan, H. L., Liu, K. P., Caracciolo, A. & Casavecchia, P. Crossed beam polyatomic reaction dynamics: recent advances and new insights. *Chem. Soc. Rev.* **46**, 7517–7547 (2017).
26. Camden, J. P., Bechtel, H. A. & Zare, R. N. Dynamics of the simplest reaction of a carbon atom in a tetrahedral environment. *Angew. Chem. Int. Ed.* **42**, 5227–5230 (2003).
27. Camden, J. P., Bechtel, H. A., Brown, D. J. & Zare, R. N. Effects of C-H stretch excitation on the H + CH_4 reaction. *J. Chem. Phys.* **123**, 134301 (2005).
28. Camden, J. P. et al. H + CD_4 abstraction reaction dynamics: excitation function and angular distributions. *J. Phys. Chem. A* **110**, 677–686 (2006).
29. Hu, W. et al. H + CD_4 abstraction reaction dynamics: product energy partitioning. *J. Phys. Chem. A* **110**, 3017–3027 (2006).
30. Pan, H. et al. Velocity map imaging study of the reaction dynamics of the H + CH_4 → H_2 + CH_3 reaction: the isotope effects. *J. Phys. Chem. A* **118**, 2426–2430 (2014).
31. Zhang, W. et al. Depression of reactivity by the collision energy in the single barrier H + CD_4 → HD + CD_3 reaction. *Proc. Natl. Acad. Sci. USA* **107**, 12782–12785 (2010).
32. Chen, W. et al. Crossed molecular beam study of H + CH_4 and H + CD_4 reactions: vibrationally excited CH_3/CD_3 product channels. *Chin. J. Chem. Phys.* **30**, 609–613 (2017).
33. Welsch, R. & Manthe, U. Loss of memory in H + CH_4 → H_2 + CH_3 state-to-state reactive scattering. *J. Phys. Chem. Lett.* **6**, 338–342 (2015).
34. Zhao, B. & Manthe, U. Eight-dimensional wave packet dynamics within the quantum transition-state framework: state-to-state reactive scattering for H_2 + CH_3 ⇆ H + CH_4. *J. Phys. Chem. A* **124**, 9400–9412 (2020).
35. Ellerbrock, R., Zhao, B. & Manthe, U. Vibrational control of the reaction pathway in the H + CHD_3 → H_2 + CD_3 reaction. *Sci. Adv.* **8**, eabm9820 (2022).
36. Xie, Z., Bowman, J. M. & Zhang, X. Quasiclassical trajectory study of the reaction H + CH_4(v_3 = 0, 1) → CH_3 + H_2 using a new ab initio potential energy surface. *J. Chem. Phys.* **125**, 133120 (2006).
37. Espinosa-Garcia, J. & Bonnet, L. Theoretical simulation of experimental imaging results for the isotopic H + CH_4/CD_4 reactions. *Theor. Chem. Acc.* **137**, 147 (2018).
38. Zhao, B. The symmetric C–D stretching spectator mode in the H + CHD_3 → H_2 + CD_3 reaction and its effect on dynamical modeling. *Phys. Chem. Chem. Phys.* **23**, 12105–12114 (2021).
39. Welsch, R. & Manthe, U. Full-dimensional and reduced-dimensional calculations of initial state-selected reaction probabilities studying the H + CH_4 → H_2 + CH_3 reaction on a neural network PES. *J. Chem. Phys.* **142**, 064309 (2015).
40. Imre, D., Kinsey, J., Sinha, A. & Krenos, J. Chemical dynamics studied by emission spectroscopy of dissociating molecules. *J. Phys. Chem.* **88**, 3956 (1984).
41. Zhao, Z., Zhang, Z., Liu, S. & Zhang, D. H. Dynamical barrier and isotope effects in the simplest substitution reaction via Walden inversion mechanism. *Nat. Commun.* **8**, 14506 (2017).

42. Eppink, A. T. J. B. & Parker, D. H. Velocity map imaging of ions and electrons using electrostatic lenses: application in photoelectron and photofragment ion imaging of molecular oxygen. *Rev. Sci. Instrum.* **68**, 3477–3484 (1997).
43. Lin, J. J., Zhou, J., Shiu, W. & Liu, K. Application of time-sliced ion velocity imaging to crossed molecular beam experiments. *Rev. Sci. Instrum.* **74**, 2495–2500 (2003).
44. Yang, X. & Liu, K. *Modern Trends in Chemical Reaction Dynamics*. (World Scientific, 2004).
45. Palma, J. & Clary, D. C. A quantum model Hamiltonian to treat reactions of the type $X + YCZ_3 \rightarrow XY + CZ_3$: application to $O(^3P) + CH_4 \rightarrow OH + CH3$. *J. Chem. Phys.* **112**, 1859–1867 (2000).
46. Peng, T. & Zhang, J. Z. H. A reactant-product decoupling method for state-to-state reactive scattering. *J. Chem. Phys.* **105**, 6072–6074 (1996).
47. Levine, R. D. *Molecular Reaction Dynamics*. (Cambridge University Press, 2005).
48. Li, J. et al. A permutationally invariant full-dimensional ab initio potential energy surface for the abstraction and exchange channels of the $H + CH_4$ system. *J. Chem. Phys.* **142**, 204302 (2015).
49. Tan, Y. et al. Revealing umbrella bending as a reporter mode in the $D + CH_4$ reaction. *Figshare*, https://doi.org/10.6084/m9.figshare.28729247 (2025).

Acknowledgements

This work was supported by the National Natural Science Foundation of China (Grant Nos. 22125302 (X.W.), 22288201 (D.Z.), 22241301 (B.Z., T.Y.), and 22327801 (X.W.)), the Guangdong Science and Technology Program (Grant Nos. 2019ZT08L455 and 2019JC01X091 (X.Y.)), the Strategic Priority Research Program of the Chinese Academy of Sciences (XDB0970100 (X.W.), XDB0970200 (D.Z.)), the Innovation Program for Quantum Science and Technology (Grant No. 2021ZD0303304 (X.Y.), 2021ZD0303305 (D.Z.)). We are gratefully indebted to Shihao Li, Yiyang Shu, Zhibing Lu, and Fuyan Wu for their assistance in experiments. We thank Hong Gao for the helpful discussions. We gratefully acknowledge the computing time supported by the Paderborn Center for Parallel Computing (PC^2) and by the Center for Computational Science and Engineering at the Southern University of Science and Technology.

Author contributions

X.Y., D.H.Z., B.Z., and X.W. conceived and supervised the research. B.Z., J.Z., Z.W., S.L., U.M., and D.H.Z. performed the quantum dynamics calculations and data analysis. Y.T., D.Y., F.L., S.Y., M.J., Y.Z., C.L., W.C., T.W., T.Y., X.Y., and X.W. performed the crossed-beam experiments. Y.T., D.Y., and X.W. performed the experimental data analysis. B.Z., X.W., D.H.Z., and X.Y. wrote the manuscript with contributions from all authors. All authors contributed to the discussions about the content of the paper.

Competing interests

The authors declare no competing interests.

Additional information

Supplementary information The online version contains supplementary material available at https://doi.org/10.1038/s41467-025-61117-1.

Correspondence and requests for materials should be addressed to Bin Zhao, Xingan Wang, Dong H. Zhang or Xueming Yang.

Peer review information *Nature Communications* thanks Björn Bastian, Gabor Czako, and the other anonymous reviewer(s) for their contribution to the peer review of this work. A peer review file is available.